FORECASTING THE PRECIPITATION ASSOCIATED WITH A MID-ATLANTIC STATES COLD FRONTAL RAINBAND

Richard H. Grumm

NOAA/National Weather Service
State College, Pennsylvania

Abstract

Hourly and 24-hour rainfall data were analyzed to document the performance of the WSR-88D rainfall algorithm and 29-km Eta model precipitation forecasts during a fast moving cold frontal rainband. The hourly rainfall observations included 100 to 150 reports per hour.

The WSR-88D precipitation algorithm underestimated the rainfall associated with the fast moving pre-frontal rainband. These errors increased with increasing range from the radar. The results show that without hourly rainfall reports available in real-time, flash flood forecasting is a difficult problem using only WSR-88D precipitation products.

Comparing observed rainfall to rainfall predictions from the 29-km Eta numerical weather prediction model revealed that the 29-km Eta model underestimated the rainfall produced by the narrow cold frontal rainband. Hourly and three-hourly data suggest that the model was too slow in moving the rainband eastward and underestimated the intensity of the rainfall rates along the rainband.

1. Introduction

On 8 November 1996, a strong cold front, with accompanying narrow and wide cold frontal rainbands, crossed central Pennsylvania and adjacent mid-Atlantic states region areas. One of the narrow cold frontal rainbands (NCFR) produced locally heavy rains, flooding, damaging surface winds, and several small short-lived tornadoes (Forbes et al. 1998). A second NCFR formed later in the day over Maryland and Virginia producing similar weather along its path. The NCFRs observed on 8 November formed along the approaching surface cold front. Over central Pennsylvania, the precipitation cores appeared to slowly outrun the surface front and weaken. New, more intense, bands then formed along the advancing cold front. This process repeated itself at least two times on 8 November 1996.

A narrow cold-frontal rainband is typically a few kilometers wide and straddles the surface cold front (Hobbs and Persson 1982). It is often composed of separate segments, each on the order of 20 km long separated by gap regions. The individual segments may contain intense precipitation cores (PCs). Areas beneath a PC may receive locally heavy rains on the order of 10-45 mm h^{-1} or more while areas in the gap regions receive precipitation on the order of 4 mm h^{-1}. The weather beneath a PC may also resemble that of a squall line. A wider band of showery and less intense precipitation may exist 50 to 100 km to the rear of this band (Matejka et al. 1980) and is referred to as the wide cold frontal rainband (WCFR). The life cycle of the NCFRs on 8 November was slightly different from those described by Hobbs and Persson (1982). However, their observations were made over the Pacific Ocean where the reduced friction may have allowed the surface front to move at a speed similar to that of the NCFR. Due to this subtle difference, we define a NCFR in the same manner as Hobbs and Persson (1982) with the exception that over the mid-Atlantic-states region weak echo gaps may develop between the traditionally analyzed frontal position and the advancing NCFR.

Relatively fast moving NCFRs can and do produce heavy rainfall despite the fact that fast moving systems are not typically associated with flash flooding. In a recent paper on ingredients-based flash flood forecasting (Doswell et al. 1996), the old axiom of where it rains the hardest the longest was reiterated as a key in forecasting locally heavy rainfall. They attributed most heavy rainfall events to copious moisture and slow moving deep convection. A fast moving cold front is not a likely candidate to produce heavy rain for a prolonged period of time. An important aspect in the short term forecasting of areas prone to heavy rain and potential flash flooding is the cell motion. The greater the motion of the cells along the line relative to the forward speed of the line, the more likely an area will receive heavy rain (see Doswell et al. 1996 Figs 3 and 4). The precipitation cores along NCFRs tend to move at an angle to the line, which may contribute to the locally heavy rains associated with relatively fast moving NCFRs.

Rain bands and squall lines, such as NCFRs, which form along or ahead of surface cold fronts, can and often do produce severe weather and flooding. These generally north to south oriented squall lines often contain small (~10-30 km) and large (~100 km) bow echo signatures (Przybylinski 1995). When these squall lines produce large areas of wind damage along their path, they are classified as serial derechos (Johns and Hirt 1987). In the mid-Atlantic states region many NCFRs may also meet the criteria of Johns and Hirt (1987) and qualify as serial derechos. A summary of the anomalous high surface temperatures and dewpoints associated with a cool season serial derecho can be found in Duke and Rogash (1992).

Operationally, forecasting the evolution of an NCFR and the accompanying rainfall is a difficult problem. During this event, the highest resolution numerical weather prediction model data available was from the

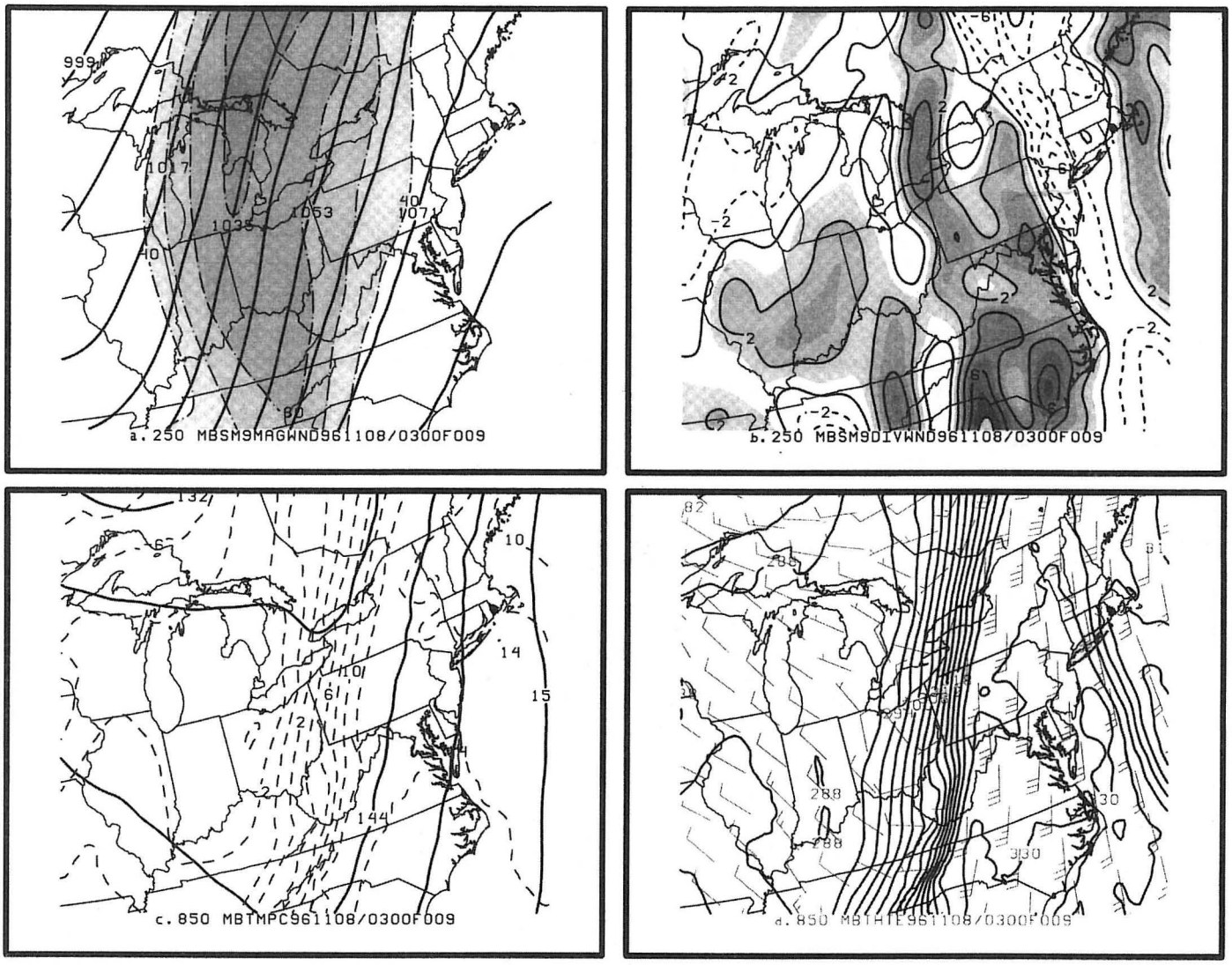

Fig. 1. Meso Eta 9-hour forecasts from the 0300 UTC 8 November 1996 forecast cycle showing a) 250 hPa height (dm) and isotachs (kt), b) 250 hPa divergence (s^{-1}), c) 850 hPa heights and isotherms (°C), and d) 850 hPa winds and equivalent potential temperature (°K). The time and date of the forecast cycle and the forecast length are displayed in each panel. The 250 hPa height contours are every 9 dm, isotach contours and shading are every 10 kt above 40 kt. Divergence contours are every 2 x 10^{-5} s^{-1} solid contours show divergence and dashed contours show convergence with shading for divergence greater than or equal to 2 x 10^{-5} s^{-1}. The 850 hPa heights are contoured every 6 dm and isotherms are every 2°C. The 850-mb equivalent potential temperatures are every 2°K with winds in kt.

NOAA/National Weather Service National Centers for Environmental Prediction (NCEP) 29-km Eta (MESO; Black 1994). The frontal circulation was approximately 200 km wide, and was resolvable by the model. However, the scale of the NCFRs is on the order of 10-20 km wide, which would require a mesoscale model on the order of 2-3 km to resolve. The MESO is capable of explicitly forecasting the precipitation associated with the broader frontal circulation, but not the precipitation associated with the NCFR. The latter produces large amounts of rainfall in short periods of time. Despite these limitations, operational forecasts of quantitative precipitation and statements related to flash flooding must be issued. Therefore, it is useful to know the limitations of the operational models and the unique situations where the forecaster can anticipate higher rainfall than forecast by the model.

The purpose of this paper is to *document* the NCFR of 8 November 1996 and the limitations of the Weather Surveillance Radar - 1988 Doppler (WSR-88D) and operational Eta models (Black 1994) associated with this event. Only one event is shown, however, data from similar events is presented to demonstrate that this is not a unique event. This paper is divided into six sections. The second section presents the data used in this study, while the third section provides an overview of the meteorological setting. The results are presented in section four. These results are discussed in section five and a brief summary of the findings is presented in section six.

2. Method

The model data used in this study includes grid point data from the operationally available NCEP MESO

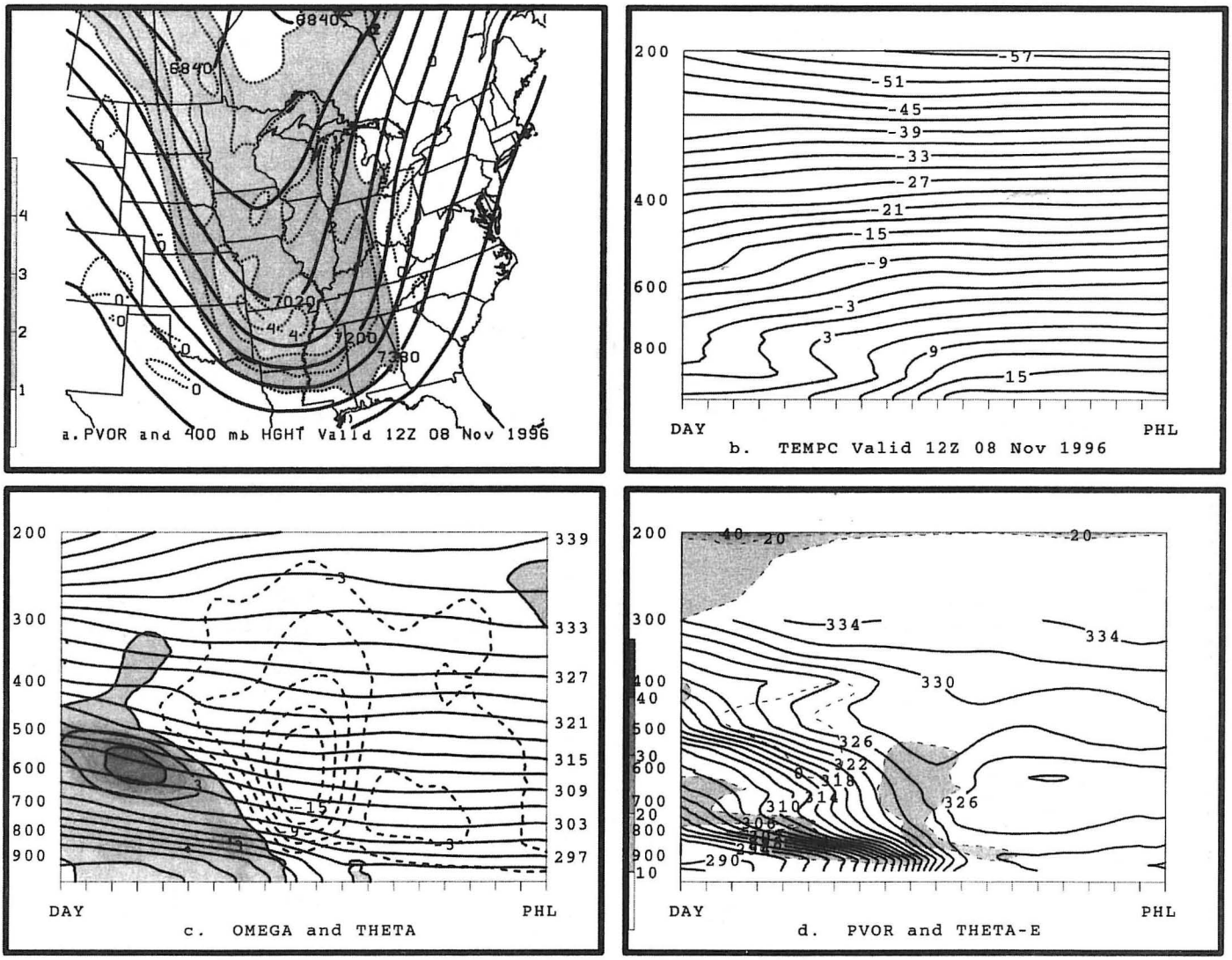

Fig. 2. As in Fig. 1 except showing a) 400 hPa heights (dm) and 500-200 hPa potential vorticity (PV; 1 PV unit is 10^{-6} km^2 kg^{-1} s^{-1}), b) isotherms (°C), c) potential temperature and omega (μs^{-1}), and d) equivalent potential temperature and potential vorticity. The cross sections were taken from Dayton, OH (DAY) to Philadelphia, PA (PHL). All temperature values are contoured at 3-degree intervals, PV in 1 PV intervals with shading denoting values greater than 1 PV unit and omega every 3 μs^{-1} with shading denoting descent.

(Black 1994). All model data were examined using GEMPAK 5.4 (desJardines et al. 1991). The 8 November NCFR was a fast moving mesoscale event and only short term forecasts, defined as forecasts less than or equal to 21 hours in length, were evaluated. This time period was chosen based on the model forecast cycles. A new model forecast cycle is typically available within 18 hours of the previous forecast cycle.

The precipitation forecasts were taken from the 0300 and 1500 UTC MESO model runs on 08 November 1996. Precipitation forecasts from the operational 80-km Eta were used to show the impact of model resolution on the forecast. An attempt was made to evaluate the 3-hourly forecasts and "storm total" rainfall produced by the model. All references to valid times will be stated as the day and time, so a forecast valid at 1200 UTC 8 November 1996 will be referred to as 08/1200 UTC.

All radar data was obtained from the central Pennsylvania (KCCX) WSR-88D. The WSR-88D archive IV products, including the one-hour (OHP) and the storm total precipitation products (STP) were examined along with the base reflectivity data. A description of these precipitation products and other WSR-88D products can be found in Klazura and Imy (1993).

Hunter (1996) reviewed errors and limitations of the WSR-88D Precipitation Processing Subsystem (PPS). Some "radar only" based errors included the radar "Delta System Calibration" (DB), attenuation, anomalous propagation, beam blockage, and range effects. During this event, the two most significant radar problems were likely the system DB and range effects. The heavy rain during this event was associated with low-topped convection. Therefore, at longer ranges the radar should underestimate the rainfall due to overshooting the highly reflective PCs. The low-topped nature may also have impacted the hybrid scan used to compute rainfall rates (Hunter 1996) at longer ranges.

Hourly and 24-hour precipitation data were obtained

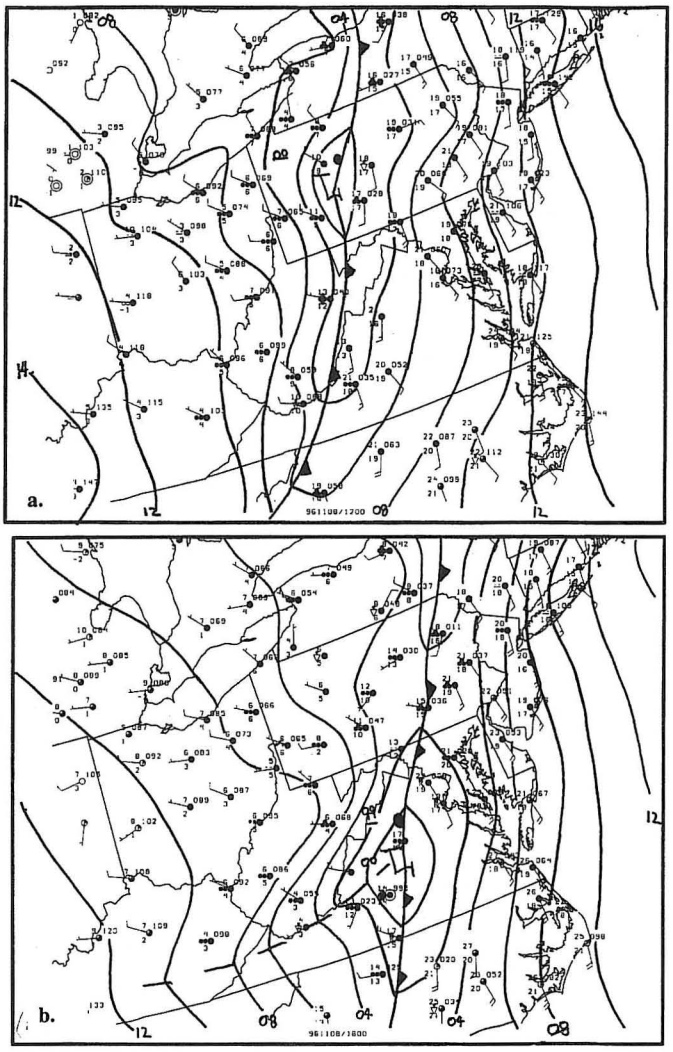

Fig. 3. Manually analyzed surface charts valid at a) 1200 and b) 1800 UTC 8 November 1996. Isobars are contoured in 2-mb increments and standard frontal symbols are used.

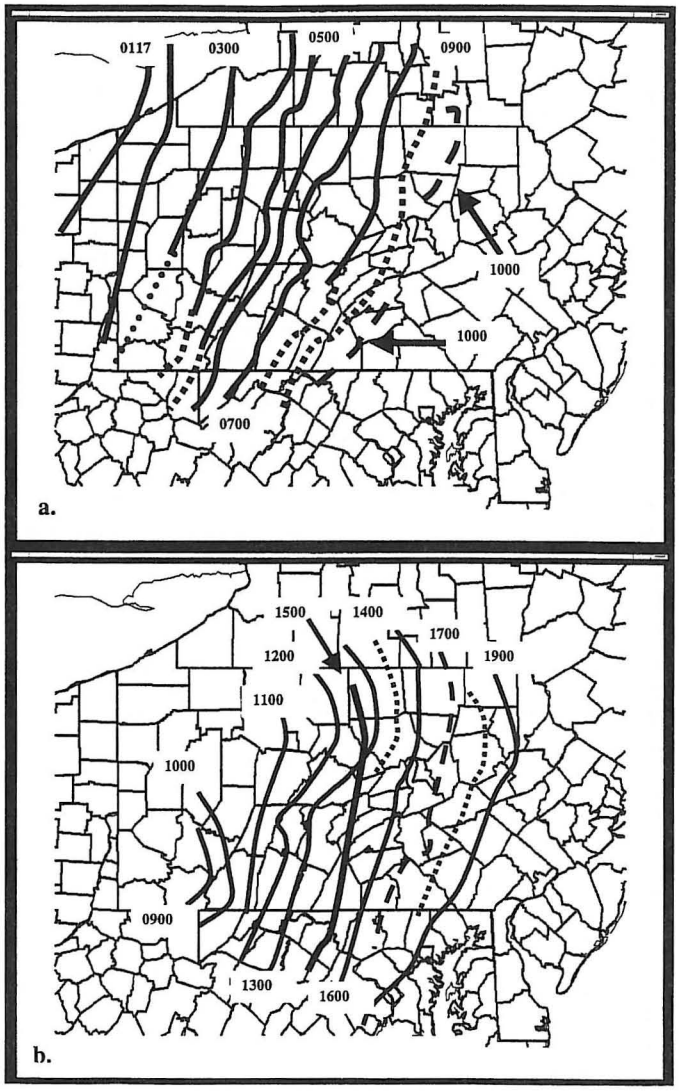

Fig. 4. Isochrones of the centroid of maximum radar reflectivity associated with the rainbands that moved across Pennsylvania between 0100 and 1900 UTC 8 November 1996. Panel a) shows the advancement of the first rainband to cross the State and b) shows the advancement of the second rainband to cross the State. Solid lines depict well-defined echo cores in excess of 30 dBZ; dashed lines depict broken lines with only a few embedded areas of echo cores in excess of 30 dBZ. The solid line appearing at 1900 UTC in panel "b" represents a third reformation of a cold frontal rainband. This band was not tracked beyond its initial formation.

from the NOAA/NWS Middle Atlantic River Forecast Center data archive. The 24-hour data include a combination of cooperative observations and automated rain gauges. Automated rain gauges are composed of Integrated Flood Observing and Warning System (IFLOWS) tipping bucket gauges; GOES Data Collection Platforms (GOES-DCP) tipping bucket and weighing type gauges; and Fischer and Porter weighing type gauges with Limited Automatic Remote Collection telemetry (LARC). The hourly data are retrieved from the IFLOWS and GOES Data Collection Platforms. Most of the hourly data are available in near real-time, approximately 15 minutes after the hour, every hour. These data are used operationally to determine the accuracy of WSR-88D precipitation estimates. Both the IFLOWS (tipping bucket gauges) and GOES-DCP (tipping buckets or weighing type gauges) are prone to underestimation errors during periods of intense rainfall and high winds (Linsley et al. 1982). Specifically, an 8 m s^{-1} wind will reduce collection efficiency by 20%, leading to an underestimation error. Similarly, as the rainfall rate increases, the tipping rates of the gauge can contribute to underes-

Table 1. Rain gauge measurement precision (mm) as a function of gauge type. A brief description of each type is provided in the text.

Gauge Type	*Precision (mm)*
IFLOWS	1.0
LARC	2.0
GOES weighing type	2.0
GOES tipping type	0.2

timation errors (Alena et al. 1990). All observed precipitation data are formatted and put into GEMPAK 5.4 surface files for plotting. Three-hourly data are derived by summing up the hourly data over the appropriate time range.

In an attempt to quantify the radar precipitation estimates and the model forecast errors, gauge-radar (G/R) and gauge-model forecast (G/F) pairs were evaluated (see Wilson and Brandes 1979). Due to irregular spacing and gaps in the gauge data, the values were not gridded. Point verification was done using locations with reliable gauges. A one-to-one gauge to radar estimation value was used. The radar estimate was rounded to the highest value in the gated estimate range. In areas where the radar overestimated (underestimated) the rainfall rate, the G/R relationship would be less (greater) than one. A preliminary WSR-88D rainfall study conducted by Klazura and Imy (1995) showed that the G/R ratio for convective rainfall was typically near or slightly lower than one and larger than one for stratiform events. Thus, the WSR-88D tends to overestimate convective rainfall and underestimate stratiform rainfall.

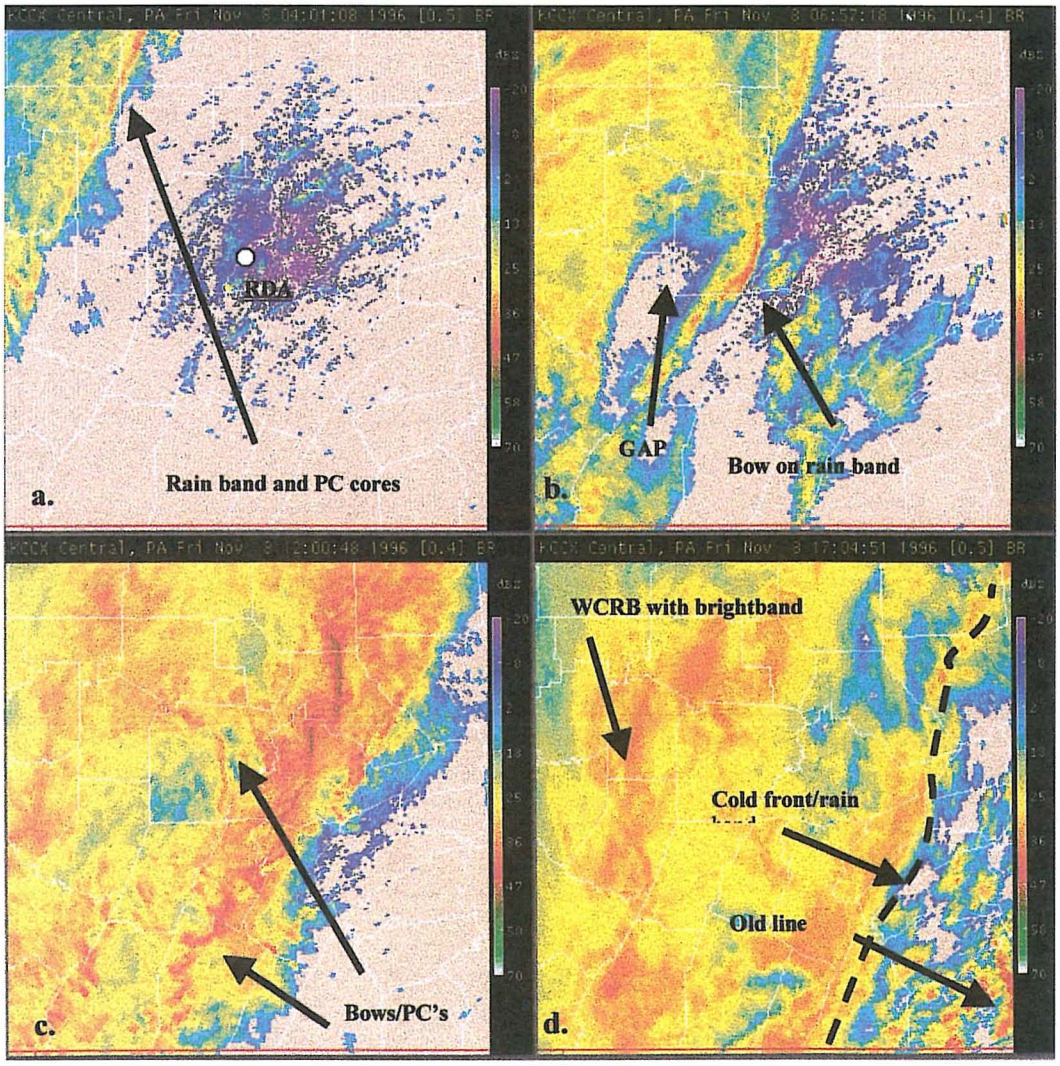

Fig. 5. WSR-88D reflectivity imagery showing the narrow cold frontal rainbands at a) 0400 UTC, b) 0657 UTC, c) 1200 UTC, and b) 1700 UTC 08 November 1996. Reflectivity scales (dBZ) are shown to the left in each panel. The location of the RDA is annotated in panel a. Significant features are also annotated.

3. Meteorological Setting

a. Synoptic setting

The large-scale setting over the mid-Atlantic states region is shown in Fig. 1. These data are 9-h forecasts from the 08/0300 UTC MESO. An examination of 08/1200 Eta and 08/1500 MESO data shows these fields to be representative. These forecast data are shown because they were the last operationally available data from which a forecast could be made prior to the event. At 250 hPa, broad southwesterly flow and a jet entrance region were forecast to move across the area (Fig. 1a). A broad area of divergence can be seen in Fig. 1b. At 850 hPa, a strong cold front can be seen in both the isotherms (Fig. 1c) and the equivalent potential temperature fields (Fig. 1d). Low-level southerly winds ahead of the front backed to westerly behind the front.

The 400 hPa heights and potential vorticity (PV; 1 PV unit is 10^{-6} km^2 kg^{-1} s^{-1}) in the 500-200 hPa layer, valid at 08/1200, are shown in Fig. 2a. These data show that a synoptic scale trough was moving eastward across the central United States, taking on a negative tilt as the short wave, as depicted by the PV field, moved through the base of the trough. Broad southwesterly flow was present over the mid-Atlantic-states region.

Regional surface analyses over the mid-Atlantic states region at 1200 and 1800 UTC 8 November 1996 are shown in Fig. 3. At 1200 UTC, a north-south oriented cold front extended from southern Canada southward through western New York, Pennsylvania, and into the Carolinas. The coarse, synoptic scale data suggests the presence of a wave along the front in southwestern Pennsylvania. By 1800 UTC, the front had moved 200 km to the east extending from southern Canada, across eastern New York into the Carolinas.

A series of cross-sections taken orthogonal to the surface front and across Pennsylvania valid at 1200 UTC 8 November 1996, are shown in Figs. 2b-d. Figure 2b

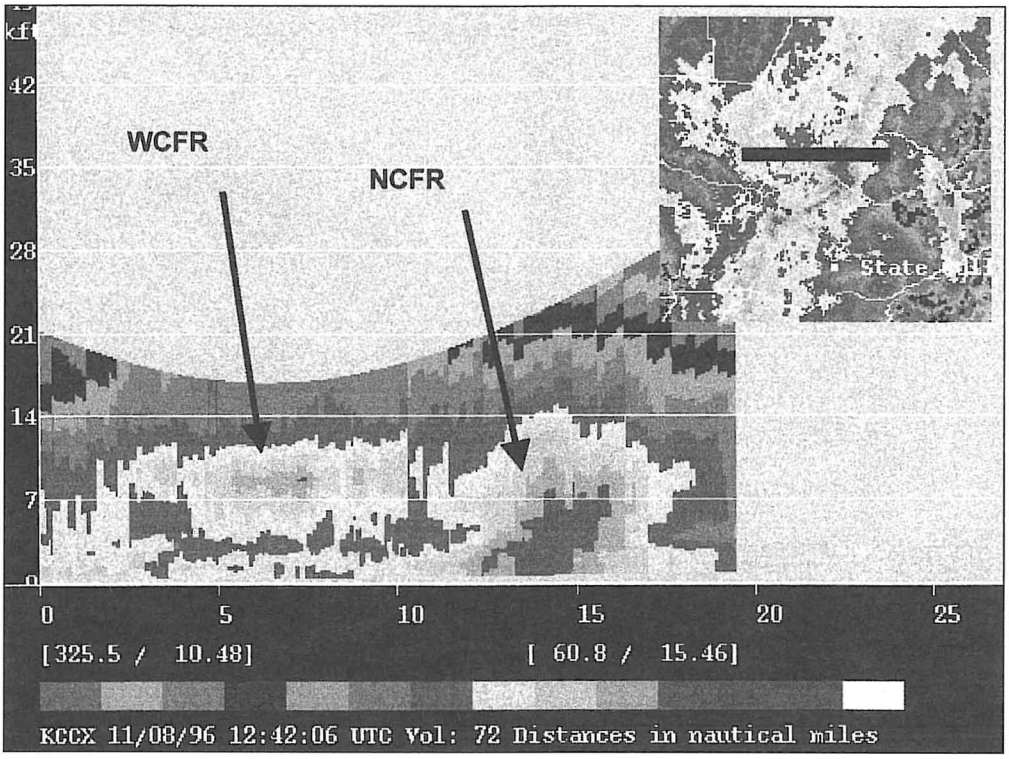

Fig. 6. A reflectivity cross section taken orthogonal to the narrow cold frontal rainband at 1242 UTC 8 November 1996. The inset at the upper right shows the location of the cross section relative to the line. The wide (WCFR) and narrow (NCFR) cold frontal rainbands are annotated in the panel.

shows the isotherms. These data show an elevated frontal boundary at 780 hPa over Dayton, Ohio (DAY) with the low-level frontal boundary in west-central Pennsylvania. Ahead of the front southeasterly winds dominated at lower levels, with the winds quickly veering to southwesterly (not shown). In the shallow cold air, low-level winds were from the northwest.

The potential temperature and vertical velocities are shown in Fig. 2c. These data also show the strong frontal boundary over central Pennsylvania with ascent (descent) on the warm (cold) side of the frontal boundary. The descent along the frontal boundary at 550 hPa over DAY sloped downward to the surface over western Pennsylvania. The circulation vectors (not shown) showed strong easterly flow up the frontal boundary, subsidence at mid-levels in the cold air, and strong low-level convergence at the leading edge of the frontal boundary. Cross-sections of frontogenesis (not shown) showed strong low-level frontogenesis in this convergent area. These data indicate that the MESO was able to capture the broad mesoscale frontal circulation (200-300 km wide) required to produce a "broad band" of rain along a strong cold front. It will be shown that the atmospheric response was on the order of a few tens of kilometers in width.

The PV and equivalent potential temperature (θ_e) for the same time period are shown in Fig. 2d. The sloped frontal surface is clearly defined in west-central Pennsylvania. The MESO forecast a slight slope over the warm air at low-levels in central Pennsylvania. The model generated relatively high (> 1 PV) PV ahead of the low-level frontal boundary and in the low-level cold air. The high PV air over Dayton at 300 hPa shows the advancing upper-level wave to the west (see Fig 2a).

b. Mesoscale setting

Isochrones of the hourly position of the NCFR are shown in Figs. 4a-b. The reformation of the NCFR along the advancing frontal boundary to the west of the original NCFR, between 0900 and 1000 UTC, necessitates the use of two panels. The NCFR was first observed by the KCCX WSR-88D shortly after 0100 UTC on 8 November 1996 over Lake Erie, extreme western Pennsylvania and northeastern Ohio. At this time, the band was along the advancing surface cold front. The band rapidly advanced across western New York and Pennsylvania during the next 7 hours. By 0300 UTC, the band began to separate from the surface front. The position of the band at 0300 UTC is in close proximity to the western edge of the Allegheny plateau. Areas to the east are generally 400 to 600 m higher than areas to the west. After 0400 UTC, the band continued to move eastward, detached from the analyzed surface frontal position. The band rapidly began to weaken and fracture after 0600 UTC and could not be tracked beyond 1000 UTC.

As the surface cold front became defined atop the Allegheny plateau, a second band began to develop along the front around 0900 UTC (Fig. 4b). This band rapidly expanded northward over the course of the next two hours as it moved eastward. Surface analysis suggests that the band remained along the front until between 1400 and 1500 UTC, when the band appeared to separate from the front. The northern segment of the band surged forward at 1400 UTC relative to the southern portion of the band. The limited surface data suggested that a wave propagated northeastward along the band. Around 1500 UTC, the northern portion of the band appeared to redevelop to the rear of the 1300 UTC position. This discrete propagation effect, centered on 1400 UTC, required the use of different line types in the figure. The heaviest rain and most of the severe weather occurred between 1200 and 1500 UTC.

Select WSR-88D radar observations of the NCFR are shown in Figs. 5a-d. At 0400 UTC (Fig. 5a) a narrow band of 30-40 dBZ cores was present northwest of the radar site. No significant radar echoes were present in the warm air ahead of this band. The clutter pattern revealed the southwest to northeast oriented ridges of

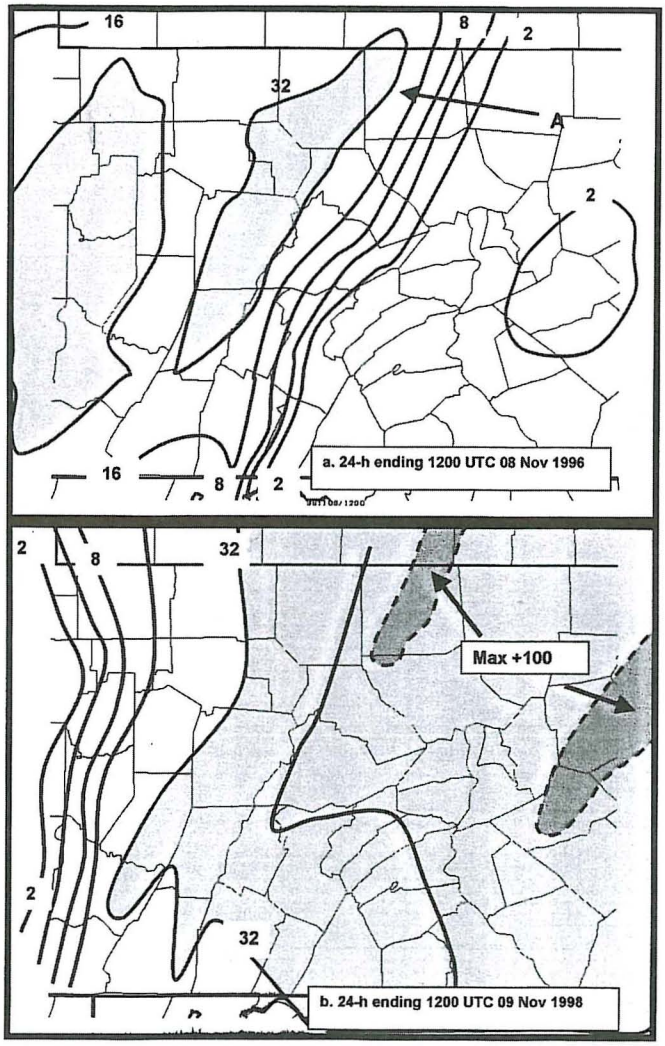

Fig. 7. Observed precipitation (mm) for the 24-hour periods ending at 1200 UTC on a) 8 November and b) 9 November 1996. Contours are powers of 2. Point "A" shows the county in which the heaviest rainfall was observed.

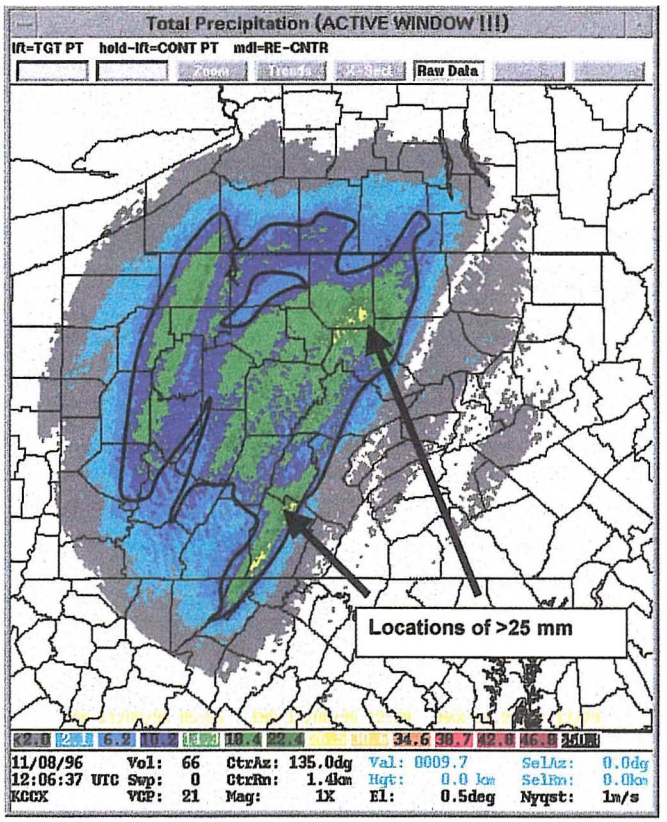

Fig. 8. KCCX WSR-88D Storm Total Precipitation (mm) valid at 1206 UTC 8 November 1996. The rainfall estimates are for the period from 0112 through 1206 UTC 8 November 1996. Shaded intervals are depicted by the key at the bottom of the image. The black contour denotes the approximate location of 10 mm of rainfall. Arrows show the location of "bright" areas of 25 mm and greater estimated rainfall.

central Pennsylvania. By 0657 UTC (Fig. 5b) the strongest echoes were along the band and a mini-bow echo structure was indicated west of the radar data acquisition site (RDA). A gap had developed between the band and the stratiform precipitation to the west. By 1200 UTC (Fig. 5c), the original band had moved eastward and was no longer discernible. Two distinct 45-55 dBZ mini bow-echoes were present just north of the RDA at this time. These features were approximately 5 km wide. The larger band, in which these features were embedded, was approximately 80 km long. By 1700 UTC (Fig. 5d), the remnants of the second band were barely discernable in the southeastern corner of the figure. A gap had developed to the west of the band. West of this gap, a more continuous area of showers and rain was present, closely aligned with the surface front. Light rain was falling to the west of the RDA. The "enhanced" echoes within the stratiform rain were due to bright band contamination in the WCFR. A reflectivity cross-section was taken orthogonal to the NCFR (Fig. 6). The intense echoes that comprised the band were only 2-5 km wide. The intense 50 dBZ echoes reached 3-4 km above the surface. A trailing area of light rain and showers, on the order of 5-10 km wide, trailed the leading band (the WCFR).

4. Results

a. Rainfall observations

The observed 24-hour precipitation over Pennsylvania, ending 08/1200 and 09/1200 UTC is shown in Figs. 7a and 7b respectively. An examination of both hourly rainfall and WSR-88D reflectivity data (not shown) suggests that the majority of the precipitation occurred along and ahead of the approaching cold front. Over western Pennsylvania, the 24-hour rainfall observed at 08/1200 occurred between 08/0300 and 08/1200 UTC. Base reflectivity data showed a well-defined NCFR moving across extreme western Pennsylvania at 08/0152 UTC (not shown). Very little precipitation was observed in the warm air east of this NCFR.

By 08/1200 UTC, most of western Pennsylvania had received 25 mm of rainfall. A small area of central Pennsylvania received in excess of 32 mm of rainfall, with a narrow core of rainfall in excess of 35 mm in north-central Pennsylvania and over the mountains of southwestern Pennsylvania. A local maximum of 44 mm was observed in

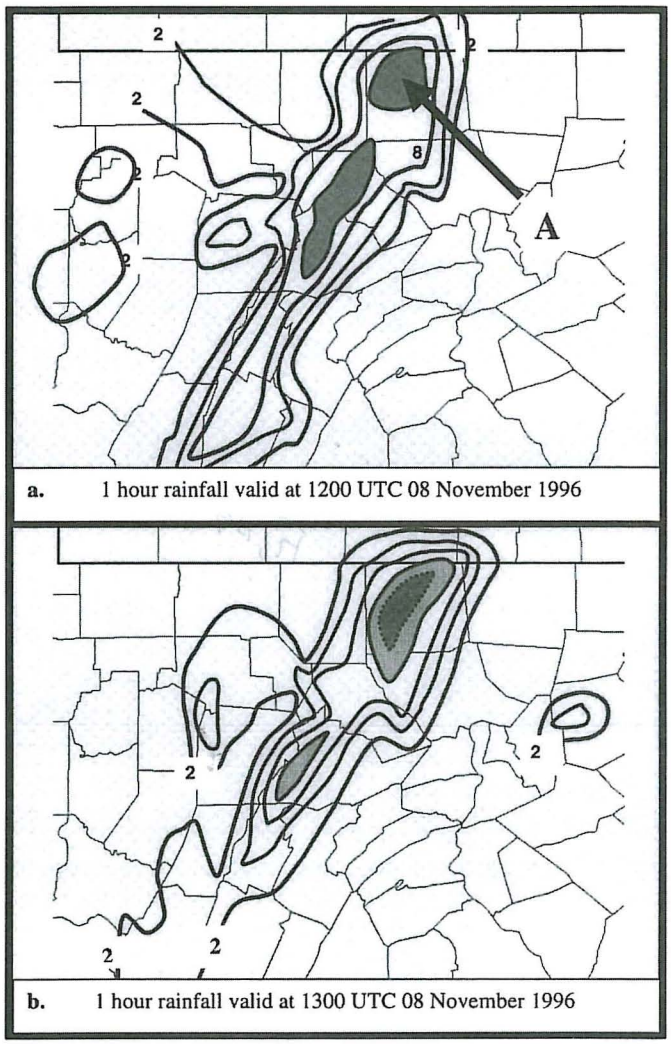

Fig. 9. Observed hourly rainfall (mm) on 8 November 1996 valid at a) 1200 and b) 1300 UTC. Contours in powers of 2. Shading denotes areas in excess of 16 mm. Point A denotes the location of heaviest rainfall.

northern Pennsylvania. Based on gauge data and spotter rainfall reports, the first Flash Flood Warning was issued at 08/1214 UTC for Tioga County (Point A), in northern Pennsylvania. The first report of flooding was received at 08/1220 UTC. Between 08/1220 UTC and 09/0000 UTC, flooding was reported in many locations in central and eastern Pennsylvania. During the day of November 8th, the maximum rainfall shifted eastward, as shown in Fig. 7b. The eastern two-thirds of Pennsylvania received greater than 20 mm of rainfall. A significant portion of eastern Pennsylvania received in excess of 80 mm of rainfall, with a few locations reporting in excess of 100 mm of rainfall. Most of the rain fell between 08/1200 and 09/0000 UTC.

b. WSR-88D rainfall estimates

The WSR-88D storm total precipitation (STP) product, valid at 08/1206 UTC, is shown in Fig. 8. The STP product shows the total estimated rainfall for the period from 08/0112 through 08/1206 UTC. The radar estimated a

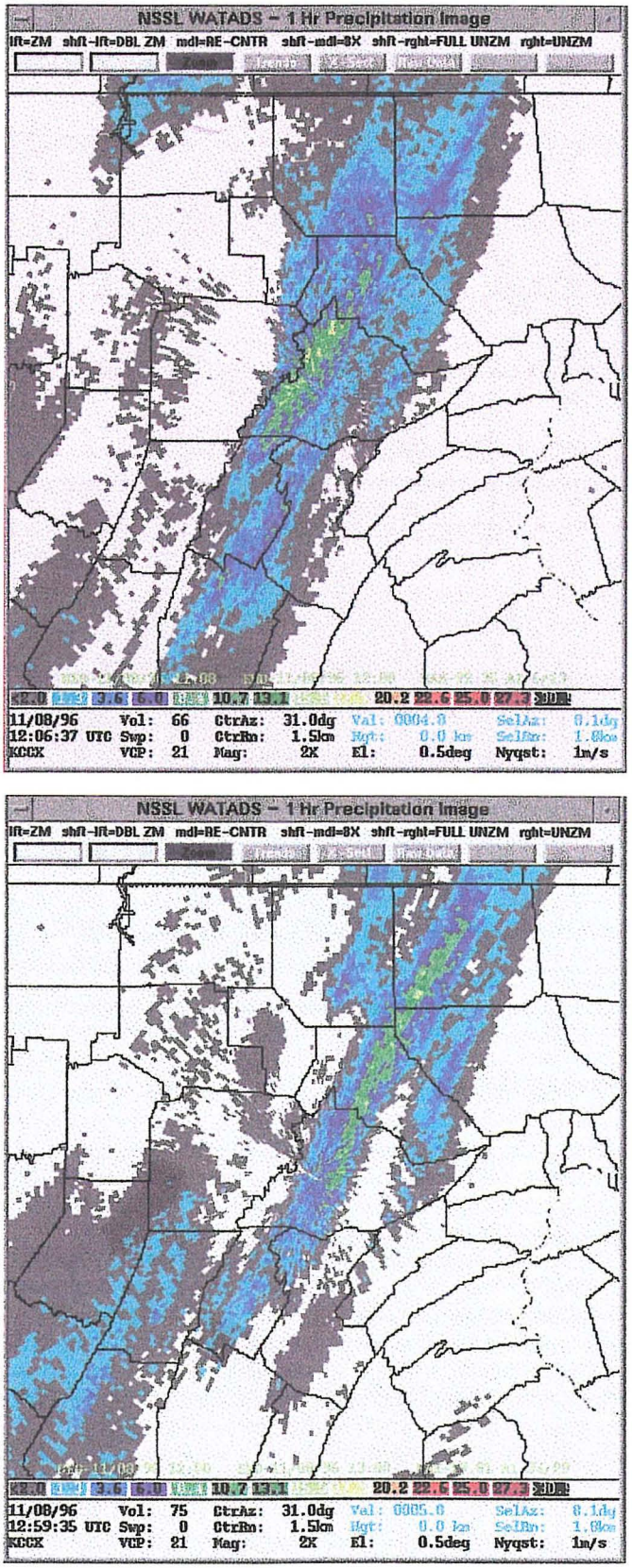

Fig. 10. WSR-88 hourly rainfall estimates (mm) valid at a) 1200 and b) 1300 UTC. The contour intervals are shown by the color key in each panel. The scale is at the bottom of the image. Bright areas along the line embedded within the darker areas represent rainfall rates of between 13 and 20 mm per hour.

large area of light rain, mainly over the western half of the state. The axis of maximum rainfall was closely aligned with the observed rainfall maximum at 08/1200 UTC (Fig. 7a). Only a few isolated locations were estimated to have received in excess of 25 mm of rainfall. Observations showed that most locations in western Pennsylvania had received more than 25 mm of rainfall (Fig. 7a). The WSR-88D STP estimates were about 50% of the observed values. At this time, and throughout the event, the WSR-88D rainfall estimates remained low relative to observed values.

An examination of hourly rainfall data showed that the heaviest rainfall was associated with the narrow line of thunderstorms as it moved eastward across Pennsylvania. Precipitation rates of 10-20 mm h^{-1} were common in association with precipitation cores along the line between 0800 and 1700 UTC. Hourly rainfall data for the periods ending at 08/1200 and 08/1300 are shown in Fig. 8. At 08/1200 UTC (Fig. 9a), the NCFR had reached its maximum horizontal length. The 10 mm contour extended from near the Maryland border northward into central New York. Along the northern half of the band two cores of greater than 15 mm of rainfall were observed in association with stronger precipitation cores. These precipitation cores were associated with embedded bow echoes. A local maximum of 23 mm of rainfall was observed at point A in Fig. 9a. By 08/1300, the rainfall decreased along the southern flank of the NCFR. Heavy rain was observed over northern Pennsylvania near point "A". This point received 23 to 37.5 mm of rain per hour between 08/1100 and 08/1400 UTC, for a 3 hourly rainfall total of 87.5 mm.

The WSR-88D hourly precipitation estimates valid at 08/1200 and 08/1300 UTC are shown in Fig. 10. At both 08/1200 and 08/1300 UTC the higher estimates were confined to the areas within 80 km of the radar. The radar estimated rainfall rates on the order of 6.25 mm h^{-1} along the NCFR with a few areas in excess of 12.5 mm h^{-1} within this area. When compared to Fig. 9, these data show that the WSR-88D underestimated the rainfall everywhere. Note that the maximum observed rainfall rates greater than 16 mm h^{-1} depicted by the shaded regions in Fig. 9. The G/R relationship along the band within 50 km of the radar was on the order of 1.25 to 1.50, indicating an underestimation of rainfall. Beyond the 50 km range ring, the G/R values were between 4.0 and 5.0. Near point "A" in Fig. 9, in excess of 120 km from the radar, rainfall totals were on the order of 20-35 mm h^{-1} while radar estimates were on the order of 2.5 to 7.5 mm h^{-1}. The G/R values in this region were generally in the 3 to 4 range. ***Overall, the radar tended to underestimate the rainfall along the main rainband.*** The most reliable estimates were obtained within 50 km of the RDA.

c. 29-km Eta model rainfall forecasts

Three hourly MESO quantitative precipitation forecasts (QPF) from the 08/0300 UTC cycle, showing the forecast valid at 9, 12, 15, and 18 hours after model initialization, are displayed in Fig. 11. These 3-h QPF reveal that the MESO forecast a broad band of rain, with an embedded more intense band, to move across Pennsylvania between 08/0900 and 08/2100 UTC. The 3-h QPF forecast valid at 08/1200 UTC (Fig. 11a) showed the axis of heaviest rainfall over northwestern Pennsylvania. The axis of heaviest rainfall moved rapidly eastward into east-central Pennsylvania by 08/2100 UTC (Fig. 11d). The observed 3-h rainfall, valid at the same times, is displayed in Fig. 12. ***These data show that the MESO underforecast the rainfall rates and was too slow to move the rainfall eastward.***

Three hourly MESO convective precipitation forecasts from the 08/0300 UTC cycle, showing the forecast valid at 12, 15, 18, and 21 hours after model initialization, are displayed in Figs. 13. These data reveal that the MESO explicitly forecast the precipitation over western Pennsylvania between 12 and 15 UTC. During the afternoon hours (Figs. 13c & 13d) a large portion of the precipitation over eastern Pennsylvania was produced by the convective parameterization scheme (CPS).

The MESO storm total rainfall amounts, valid at 08/1200 UTC and 09/0000 UTC from the 08/0300 UTC MESO, are shown in Figs. 14a and 14b respectively. Corresponding forecasts from the Eta are displayed in Figs. 14c and 14d. These data reveal that the MESO forecast more detail than the Eta. For example, the MESO forecast a well-defined band of heavier rainfall over western Pennsylvania (Fig. 14a) relative to the broader feature forecast by the Eta (Figs. 14c) in the same region. Overall, the MESO forecasts were quite similar to the Eta forecasts despite the slightly longer period of data in the Eta. Both models picked up on the band of rain over western Pennsylvania prior to 08/1200 UTC, the precipitation minimum over West Virginia and western Maryland, and the second band of heavier rainfall over eastern Pennsylvania by 09/0000 UTC.

5. Discussion

The NCFR, which crossed central Pennsylvania between 08/0200 and 09/0000 UTC, produced a large area of 25 to 75 mm of rainfall with locally higher amounts on the order of 75-125 mm. Most of this rainfall was observed in a 3-4 hour period . Hourly rainfall rates ranged from 10 to 40 mm h^{-1} as the band crossed the state. During the 8 November event, a report of 178 mm of rain was observed over a small area in northern Pennsylvania. As described by Hobbs and Persson (1982) areas beneath PC received the highest rainfall rates. A large portion of the event total rainfall typically occurred in a short period of time, likely associated with passage of a PC along the NCFR. Due to the short duration of the heavy rainfall, NCFR events tend to produce urban and small stream flooding. The high rainfall amounts observed on 8 November produced flooding along streams and rivers in central Pennsylvania.

Using the hourly and the 24-hour precipitation data, an evaluation of WSR-88D derived precipitation products was obtained. The main WSR-88D products evaluated included the OHP and STP. Not surprisingly, the hourly data revealed that the WSR-88D underestimated the rainfall by at least a factor of 2 throughout the event. Close to the radar, the estimates were more reliable and the validity of the estimates decreased with increasing range.

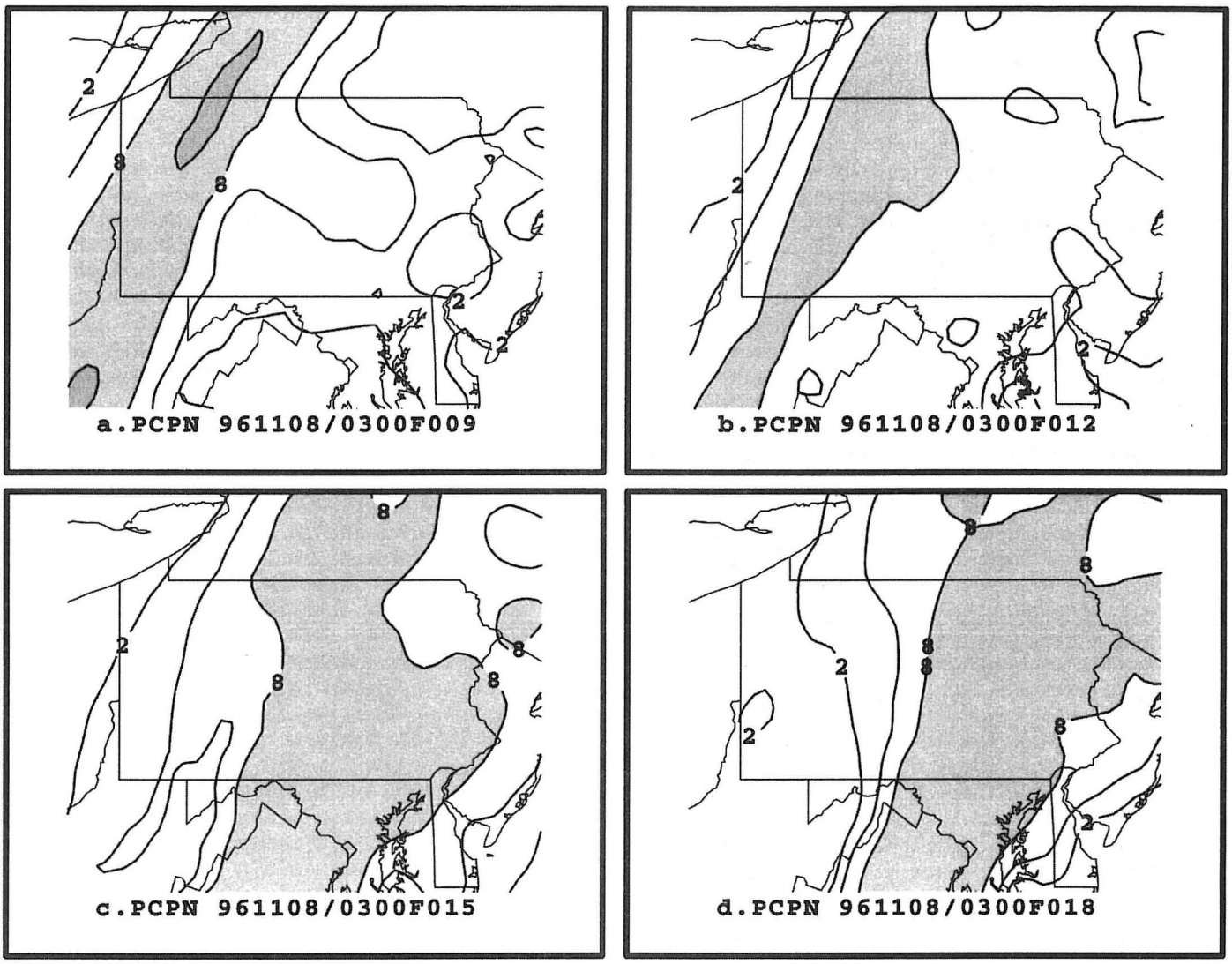

Fig. 11. Three-hour quantitative precipitation forecasts (mm) from the 0300 UTC 8 November 1996 forecast cycle of the 29-km Eta valid at a) 1200, b) 1500, c) 1800, and d) 2100 UTC 8 November 1996. Precipitation is contoured in powers of 2 mm with shading to denote values in excess of 8 mm of precipitation.

There are many factors that likely contributed to the radar precipitation underestimates. Some of the more significant factors in this event were probably related to the low-topped nature of the convection and the WSR-88D PPS (Hunter 1996). Klazura and Imy (1995) showed that with stratiform precipitation, WSR-88D precipitation estimates tended to underestimate rainfall at longer ranges due the radar beam overshooting the precipitation cores. In the absence of bright banding, a similar error would be expected with most low-topped convection. During this event, the radar detected reflectivity cores of 50-60 dBZ along the NCFR. These cores were observed at or below 1 km in elevation. Few cores in excess of 50 dBZ were observed beyond 100 km from the radar. At longer ranges (beyond 90 km) reflectivity values rarely ranged higher than 30 to 40 dBZ, implying the radar beam overshot the strongest precipitation cores.

The operational implications of the errors in the WSR-88D PPS are that a G/R relationship should be established and monitored during precipitation events. Determining a G/R relationship requires timely and accurate hourly rainfall data. Unfortunately, reliable hourly data are not always available. Although the WSR-88D underestimated the rainfall throughout the event, it did an excellent job depicting the axis of maximum rainfall. This information and rain gauge data can be used to establish representative G/R relationships by range. A representative G/R relationship could be used to correct WSR-88D rainfall estimates (Fulton 1999).

A comparison of MESO QPF to observed rainfall data revealed that the model was unable to forecast the observed rainfall rates. There appeared to be a timing error, with the MESO being too slow in moving the precipitation eastward. Although these errors are operationally significant, they are more likely related to the model resolution (29 km) relative to the scale of the heavy rain producing NCFR (~20 km). From a scale consideration, the MESO should have a high probability of forecasting phenomena on the order of 6Δ, where Δ is the model horizontal grid scale. In this case, the MESO had

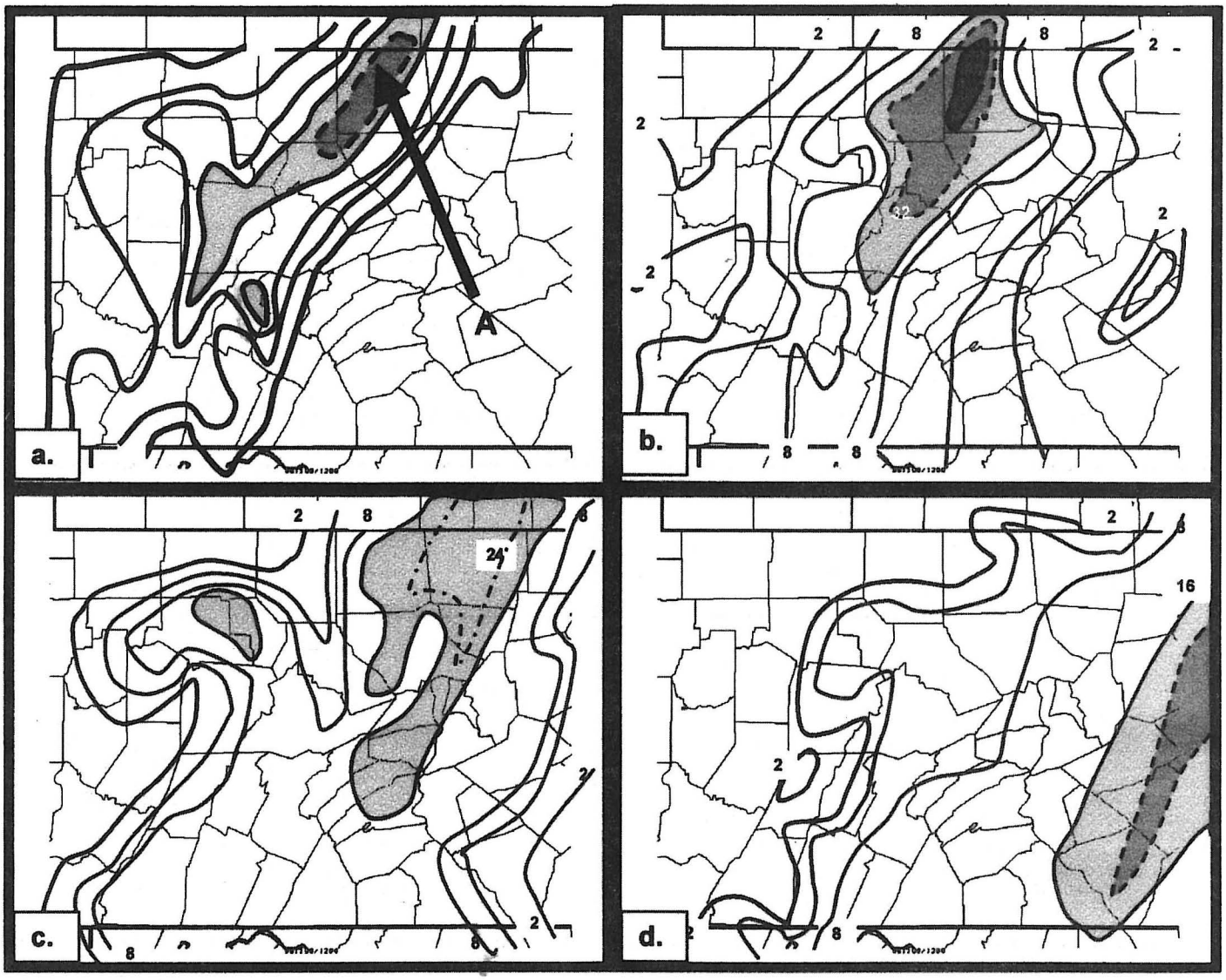

Fig. 12. As in Fig. 9 except for 3-hour observed rainfall (mm) valid at a) 1200 UTC, b) 1500 UTC, c) 1800 UTC and d) 2100 UTC 08 November 1996.

a reasonable chance of forecasting meteorological phenomena on the order of 180 km. This was close to the scale of the cold frontal circulation diagnosed by the MESO (see Fig. 2). A mesoscale model on the order of 3 km would be required to properly simulate an NCFR.

The scale of the MESO frontal circulation (~200 km) and the broad area of precipitation the model generated (~200 km) suggest that the model correctly forecast a strong cold frontal circulation. Unfortunately, the model response was a broad area of precipitation, which straddled the front. Initially, the models explicitly forecast the light precipitation along and ahead of the front. After 1200 UTC, the model precipitation forecasts were dominated by the convective parameterization scheme rather than the grid scale forcing (see Fig. 13). In the atmosphere, the instability was realized in a narrow band on the order of a few tens of kilometers wide. The most intense precipitation was produced by precipitation cores on the order of only 5-10 km in width. The atmosphere released convective instability rapidly, producing localized areas of heavy rainfall. The model released convectively parameterized precipitation in the unstable warm low-level warm air ahead of the surface cold front (see Fig. 2d and Fig. 13).

Model sensitivity studies continue to show improved QPF as horizontal resolution is increased. Senesi et al. (1996) found errors similar to those shown in this study in model simulations of the Vaison-La-Romaine Flash Flood. Comparing different models with varying horizontal resolutions and convective parameterization schemes (CPSs), they noted that finer scale models made more realistic simulations of the shape and character of the rainfall patterns. The finer scale models underestimated rainfall amounts in the higher ranges (greater than 70 mm) while the coarser resolution models underestimated rainfall at lower ranges (greater than 20 mm). Using the 10 km Peridot model, they were able to forecast a 200 mm precipitation maximum within 30 km of an observed maximum of 300 mm. They found: 1) that the higher resolution models more accurately forecast the

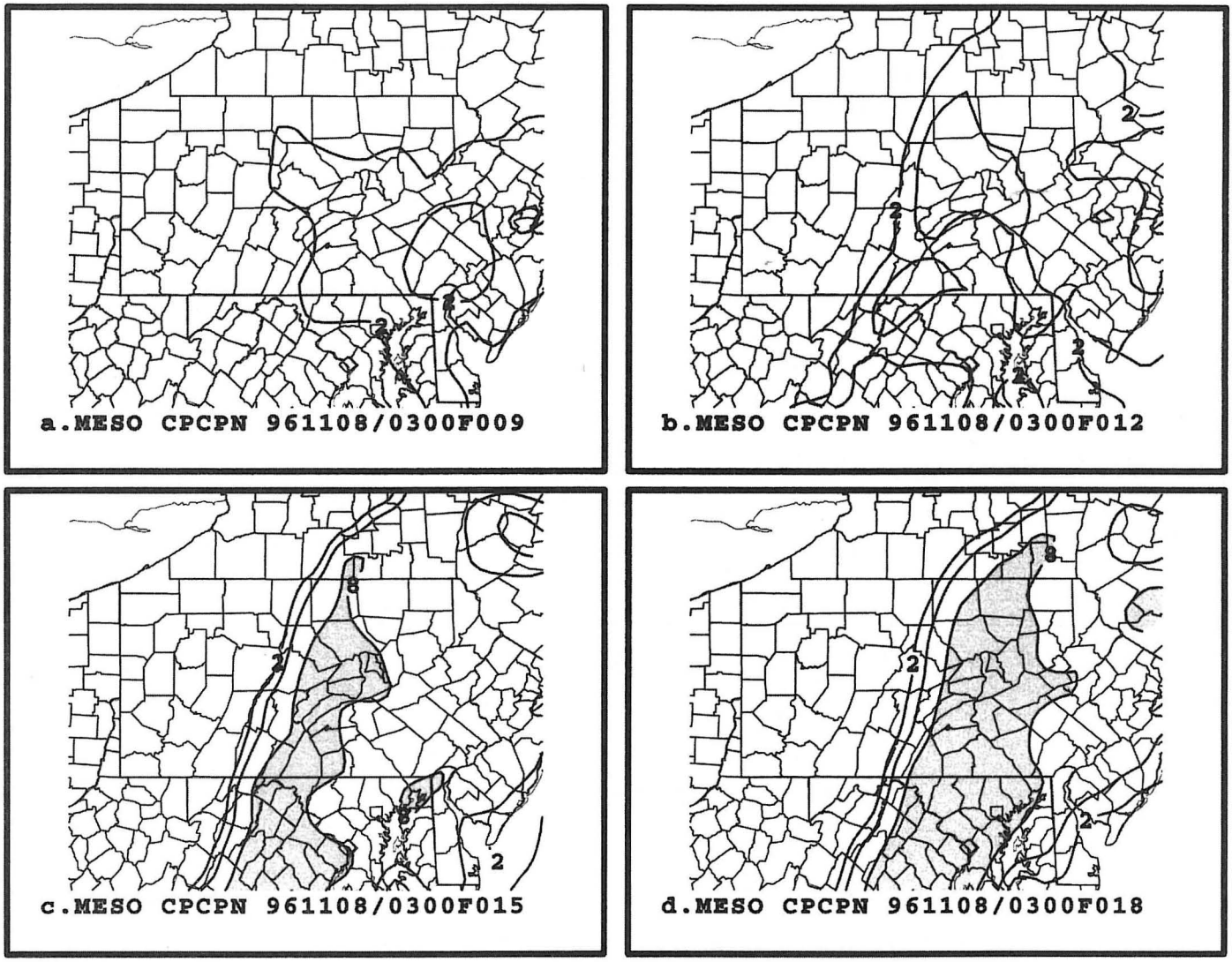

Fig. 13. As in Fig. 11 except showing 29-km Eta convective precipitation.

amount and location of the precipitation maximum, 2) that all the models were too slow to move the precipitation eastward, and 3) that fine resolution mesoscale models will improve QPFs.

In a more recent study, Gallus (1999) used the operational Eta model to forecast the rainfall associated with two heavy rainfall events over Iowa. Simulations were run at 22, 39, and 78 km. All versions of the model had 32 vertical layers. The model simulations showed that as the horizontal grid resolution was increased, the model forecast more precipitation. For several cases, a special 12-km run was made. Peak precipitation amounts for the event ranged from 10 mm of rainfall at 78 km to 203 mm at 12 km. At the 78 and 39-km scale, 90% of the precipitation came from the convective parameterization scheme. At finer resolutions, approximately 30 mm of the rainfall came from the CPS, with the majority of the precipitation (173 mm) being explicitly forecast.

The results show that NCFRs, on the order of 10-20 km wide and 100 km long, may be too small scale a feature for the MESO to resolve. With a 29 km horizontal resolution, the MESO has too coarse a grid to explicitly forecast convective precipitation, relying on the CPS to produce convective rainfall. There are many issues related to the selection of the CPS in a numerical model. Wang and Seaman (1997) evaluated the 4 most commonly used CPC's using The Pennsylvania State University - National Center for Atmospheric Research mesoscale model (MM5). Their results showed that the modified Betts-Miller CPS (Janjic 1994) typically underestimated convective rainfall, especially in areas of heavy rainfall. In this event, BMJ's dependence on the stability in the lowest 130 hPa may have limited the convective response to the warm air ahead of the frontal zone.

Decreasing the models resolution to 20 km or less would allow the model to partially resolve convective elements (e.g., Weisman et al. 1997; Molanari and Dudek 1992). This poses significant questions including whether a hydrostatic or non-hydrostatic model should be used and the role the CPS would play in the model. A more difficult forecast problem is predicting the development and the motion of the smaller PC's along the NCFR. The results shown here suggest that the heaviest rain and flash flooding were associated with these intense small-

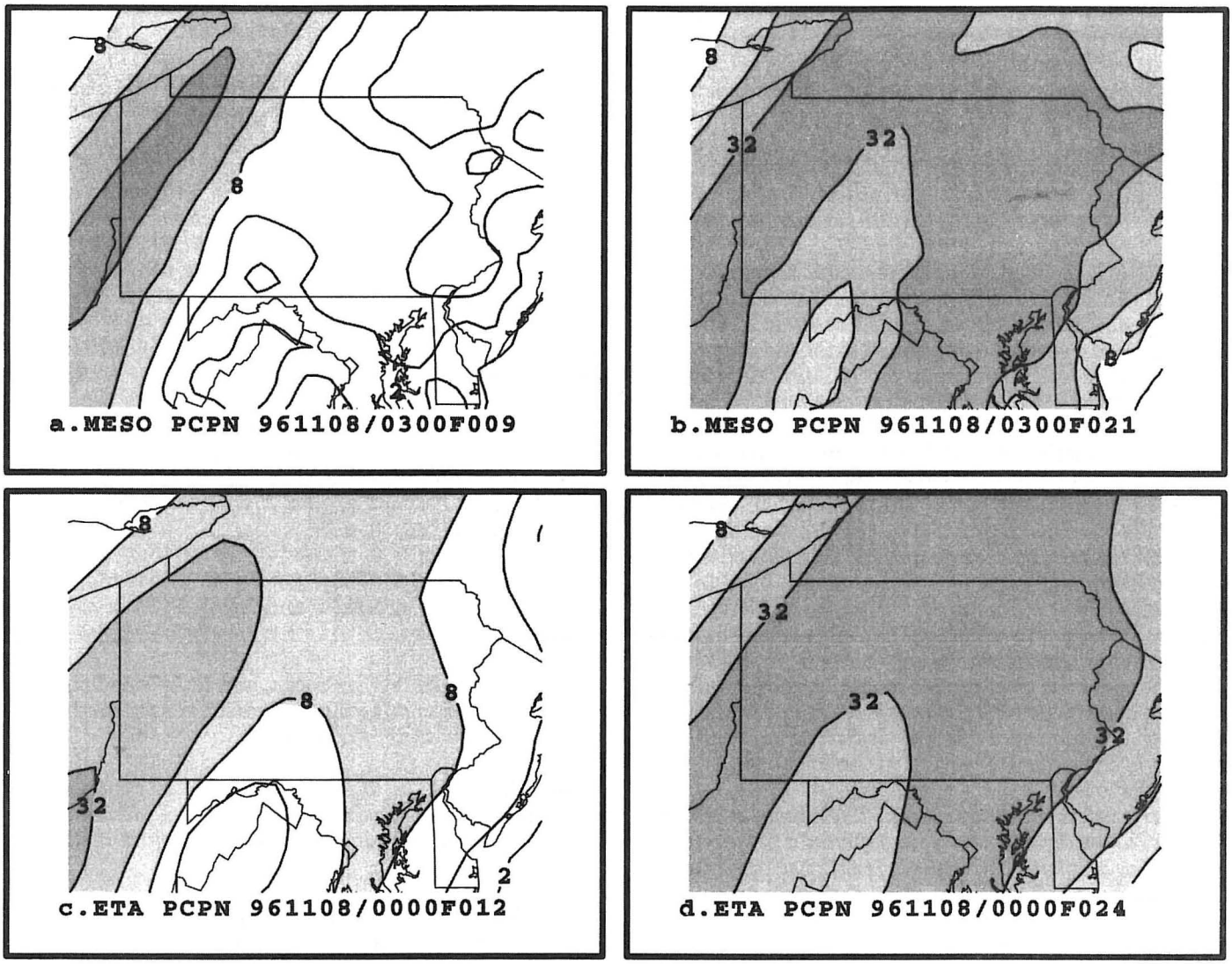

Fig. 14. As in Fig. 11 except showing 29-km Eta total precipitation valid at a) 1200 UTC 08 November and b) 0000 UTC 09 November 1996 and 80-km Eta forecasts valid at c) 1200 UTC 08 November and b) 0000 UTC 09 November 1996.

scale features. Numerical models with horizontal resolutions on the order of 8-12 km may be capable of resolving convective evolutions (Weisman et al 1997; Kato and Saito 1995) and the rainfall associated with these features. The question then is where will the detailed mesoscale models be run, at National Centers or Regional or local forecast offices?

During the 8 November 1996 NCFR event, the MESO failed to produce convective precipitation rates in excess of 16 mm $(3h)^{-1}$ during any 3-h period. An examination of several other convective rainfall cases over the northeastern United States (not shown) where implicit (subgrid scale) precipitation dominated the total forecast precipitation amounts reveals a similar 15-16 mm $(3h)^{-1}$ maximum convective rainfall limit. The most intense convective rainfall found was along the North Carolina coast during Hurricane Fran (September 1996) where the MESO produced 22 mm $(3h)^{-1}$ of convective rainfall. It is unclear why, but it appears that the MESO has an upper limit in its convective rainfall rate in the 15-16 mm $(3h)^{-1}$ range over the northeastern United States. This creates an operational QPF dilemma since the data shown here suggests the atmosphere can produce and sustain 25 mm h^{-1} rainfall rates over large areas for several hours. Furthermore, Doswell et al. (1996) defined heavy rainfall as rainfall rate in excess of 25 mm h^{-1}, a rate that the operational MESO could not produce. Based on this case, and a limited sample of cases available over the dense rainfall network, maximum convective model forecasts of rainfall rates of 15-16 mm $(3h)^{-1}$ do not provide useful flash flood forecast guidance.

6. Conclusions

Hourly and 24-hour rainfall gauge data were used to assess the WSR-88D precipitation algorithm and the MESO QPF forecasts during a fast moving NCFR event. The results show that the WSR-88D underestimated rainfall and the MESO underforecast the precipitation associated with these fast moving low-topped convective events.

The WSR-88D algorithm did an excellent job depicting the location and axis of the precipitation maximum.

However, the WSR-88D OHP and STP products underestimated the rainfall rates. Due to inherent errors in the Z-R relationship and the low-topped nature of convection in this event, radar tended to underestimate precipitation rates. This underestimation error grew larger with increasing range from the radar. ***Using rain gauge data and establishing G/R relationships at discrete range intervals provides a correction factor, which can be used to improve the radar precipitation estimates.***

The MESO tended to ***underforecast*** the maximum observed rainfall. Part of the error was due to the MESO being too slow in moving the rainfall eastward. Another part of the error seemed to be related to the inability of the CPS to produce sufficiently high precipitation rates. In no single 3-h period did the MESO produce convective or total precipitation rate in excess of 15-16 mm $(3h)^{-1}$. In addition to underforecasting the maximum precipitation cases, the MESO showed a strong bias in overforecasting the lighter precipitation cases. Throughout this event, the MESO also forecast large regions of light precipitation, 2-4 mm $(3h)^{-1}$, where little or no precipitation was observed.

The results suggest that forecasters still have to recognize meteorological patterns, which favor heavy rainfall. The current limitations of the Z-R relationship and the relatively coarse resolution, relative to mesoscale phenomena, of the operational models will often underestimate and under forecast heavy rainfall, respectively. Knowing the limitations of the observing and forecast systems is critical in improving weather forecasting and warning processes.

Future research efforts should be aimed at establishing discrete G/R relationships as a function of range to improve WSR-88D rainfall estimates. These ***"corrected"*** estimates could than be used to verify and improve mesoscale QPFs. These types of data, with hourly resolution, would be useful in isolating both precipitation spin-up and timing errors. We have examined six other NCFR cases, which revealed similar model and radar errors. In all cases, the models correctly forecast an elongated precipitation maximum (suggesting a precipitation band), but underforecast the amount and eastward progression of the precipitation. This particular event was selected due to the heavy rain, severe weather, and complete data archive. A follow-on study might include, fine scale models with grid resolutions on the order of 10 km to evaluate the impact on grid resolution on forecasting the rainfall associated with these NCFRs.

Acknowledgments

The author thanks the staff of the National Weather Service (NWS) Office in State College for collecting and archiving all significant flooding and spotter rainfall reports recorded during this event. Thanks to those who provided editorial assistance in preparing this manuscript, especially Laurie Hermes. The NWS Eastern Region and the NWS Headquarters Office of Meteorology made this research possible due to the continued support of the Scientific Applications Computer program. For help in editing and ideas on this paper, the author thanks Kevin P. Hlywiak and David L. Michaud.

Author

Richard Grumm is the Science and Operations Officer at the National Weather Service Office in State College, Pennsylvania. He previously worked in the Meteorological Operations Division of the NWS National Meteorological Center (now NCEP) in Camp Springs, Maryland. His primary interests include evaluating numerical model performance and major eastcoast snowstorms. He received his B.S. (1979) from the State University of New York at Oneonta and his M.S. (1981) from the State University of New York at Albany.

References

Alena, T. R., J. S. Appleton and W. H. Serstad, 1990: Measurement accuracy of tipping bucket rain gauges at high rainfall rates. Preprints, *Conf. on Operational Precipitation Estimation and Prediction*, Anahiem, CA, Amer. Meteor. Soc., 16-19.

Black, T. L., 1994: The new NMC mesoscale model: Description and forecast example. *Wea. Forecasting*, 9, 265-278.

Doswell, C. A. III, H. E. Brooks, and R. A. Maddox, 1996: Flash flood forecasting: An ingredients-based methodology. *Wea. Forecasting,* 11, 560-581.

desJardines, M. L., K. F. Brill and S. S. Schotz, 1991: GEMPAK5 User's Guide. *NASA Technical Memorandum 4260*, National Aeronautics and Space Administration, 2021 pp.

Duke, J. W. and J. A. Rogash, 1992: Multiscale review of the development and early evolution of the 9 April 1991 Derecho. *Wea. Forecasting*, 7, 623-635.

Forbes, G. S. M., M. L. Pearce and R. H. Grumm, 1998: Downbursts and gustnadoes from mini-bow echoes and affiliated mesocyclones over central Pennsylvania. Preprints, *16th Conf. on Weather Analysis and Forecasting*, Phoenix, AZ, Amer. Meteor. Soc., 295-300.

Fulton, R.A, 1999: A Sensitivity of WSR-88D rainfall estimates to the rain-rate threshold and rain gauge adjustments: A flash flood case study. *Wea. Forecasting*, 14, 604-624.

Gallus, W. A., Jr., 1999: Eta simulations of three extreme precipitation events: Sensitivity to resolution and convective parameterization. *Wea. Forecasting*, 14, 405-426.

Hobbs, P. V. and P. O. G. Persson, 1982: The mesoscale and microscale structure and organization of clouds and precipitation in midlatitude cyclones. Part V: The substructure of narrow cold-frontal rainbands. *J. Atmos. Sci.*, 39, 280-295.

_____, J. D. Locatelli, and J. E. Martin, 1990: Cold fronts aloft and the forecasting of precipitation and

severe weather east of the Rocky Mountains. *Wea. Forecasting*, 5, 613-626.

Hunter, S. M, 1996: WSR-88D radar rainfall estimation: capabilities, limitations and potential improvements. *Natl. Wea. Dig.*, 20:4, 26-38.

Janjic, Z. I., 1994: The step-mountain Eta coordinate model: Further developments of the convection, viscous sublayer, and the turbulence closure schemes. *Mon. Wea. Rev.*, 122, 927-945.

Johns, R. H. and W. D. Hirt, 1987: Derechos: widespread convectively induced windstorms. *Wea. Forecasting*, 2, 32-49.

Kato, T., and K. Saito, 1995: Hydrostatic and non-hydrostatic simulations of moist convection. *J. Meteor. Soc. Japan*, 73, 59-77.

Klazura, G. E. and D. A. Imy, 1995: A Comparison of high resolution rainfall accumulation estimates from the WSR-88D precipitation algorithm with rain gauge data. Preprints, *27th Int'l Conf. on Radar Meteorology*, Vail, CO, Amer. Meteor. Soc., 31-24.

_____, and _____, 1993: A Description of the initial set of analysis products available from the NEXRAD WSR-88D system. *Bull. Amer. Meteor. Soc.*, 74, 1293-1311.

Linsley, R. K., M. A. Kohler, and J. L. H. Paulhus, 1982: *Hydrology for Engineers*. McGraw-Hill, 508 pp.

Matejka, T.J., R.A. Houze, and P.V Hobbs, 1980: Microphysics and dynamics of clouds associated with mesoscale rainbands in extratropical cyclones. *Quart. J. R. Met. Soc.*, 106, 29-56.

Mesinger, F., 1996: Improvements in quantitative precipitation forecasts with the Eta regional model at the National Centers for Environmental Prediction: The 48 km upgrade. *Bull. Amer. Meteor. Soc.*, 77, 2637-2649.

Molanari, J. and M. Dudek, 1992: Parameterization of convective precipitation in mesoscale numerical models. *Mon. Wea. Rev.*, 120, 326-344.

Przybylinski, R.W., 1995: The bow echo: Observations and numerical simulations, and severe weather detection methods. *Wea. Forecasting*, 10, 203-218.

Senesi, S., P. Bougeault, J. L. Cheze, P. Cosentino, and R. M. Thepenier, 1996: The Vasion-La-Romaine flash flood: mesoscale analysis and predictability issues. *Wea. Forecasting*, 11, 417-442.

Wang, W. and N. L. Seaman, 1997: A comparison of convective parameterization schemes in a mesoscale model. *Mon. Wea. Rev.*, 125, 252-278.

Weisman, M. L., W. C. Skamarock, and J. B. Klemp, 1997: The resolution dependence of explicitly modeled convective systems. *Mon. Wea. Rev.*, 125, 527-548.

Wilson, J. W. and E. A. Brandes, 1979: Radar measurement of rainfall - A summary. *Bull. Amer. Meteor. Soc.*, 60, 1048-1059.